

Absorbing Material Characterization in a Reverberation Chamber

Emmanuel Amador, Mihai Ionut Andries, Christophe Lemoine, Philippe Besnier

Université Européenne de Bretagne

INSA, IETR, UMR CNRS 6164

Rennes, France

Email: emmanuel.amador@insa-rennes.fr

Abstract—In this paper we present an absorption model in a reverberation chamber (RC). This time domain model uses time constants measurements to characterize absorbers in reverberation chambers in a given frequency range through their absorbing cross sections. The absorption of a rectangular piece of absorber is evaluated and the effect on the loading for different configurations and with several pieces of absorber is discussed. This analysis allows a fine control of the loading of the chamber. Finally, the material of the absorbing object is characterized through an absorbing efficiency coefficient, extracted from simulations and measurements.

I. INTRODUCTION

Reverberation chambers (RC) are traditionally used for EMC tests. Their capacity to create reproducible conditions is now used to simulate communication channels for wireless devices. In order to get consistent results in EMC testings or channel simulation with different reverberation chambers, the loading of the chamber must be adjusted with precision. In EMC testings, the loading of the chamber controls its quality factor and the lowest usable frequency *i.e* the field uniformity of the chamber [1], [2], [3]. For channel simulation purposes, the loading impacts the power delay profile, a parameter that should be adjusted with precision to simulate various propagation environments [4].

In order to control precisely the loading of a chamber one should characterize the absorbing objects in the cavity first. In [5] the authors propose a theoretical model of absorption with lossy spheres and discuss the effect of the amount of similar objects on the quality factor of the chamber. In [6], the authors present several measurements that show the effect of the position of the absorber in the chamber on the loading, but the conclusion on how the absorber affects the loading of the chamber is mostly empirical.

In this paper, a simple numerical model [7] gives the theoretical background necessary to understand how the power is absorbed in an RC. With the help of this time domain model and with basic probability concepts, we construct an exponential decay model that integrates the losses through an absorbing cross section σ_a . This absorbing cross section is easily extracted from measurements of the time constants of the power decay in the empty cavity (τ_{ec}) and in presence of the absorber (τ_a). This model is applied to a rectangular piece of absorber and then to several pieces of rectangular absorbers. The impact of a pyramidal absorber on the loading

is studied. In the end we extract an efficiency coefficient that characterizes (in an RC) the absorption of the material used in the absorber.

II. ABSORBING MECHANISM IN A REVERBERATION CHAMBER

A. Exponential Model and Image Theory Model

The absorption model developed is based on an exponential model of the power received in the RC. We use a model based on image theory [7] to develop our calculations.

An RC is a microwave resonator that can be characterized for a given frequency by its quality factor Q or its time constant τ . The relation between Q and τ is given by:

$$Q = 2\pi f\tau, \quad (1)$$

where f is the operating frequency. The power received of a channel impulse response (CIR) is given by an exponential formula (the time constant τ is considered approximately constant in the frequency range):

$$P(t) = P_0 e^{-t/\tau}. \quad (2)$$

The numerical model based on image theory [7] allows to express the time constant τ as a function of a typical distance L of the chamber and a loss coefficient R that includes losses from the walls and the antennas when the chamber is empty. The amplitude of the E-field after $n + 1$ reflections can be expressed as function of the amplitude $E(n)$ of the E-field after n reflections:

$$E(n + 1) = RE(n) = R^{n+1}E_0. \quad (3)$$

The model based on image theory provides the exact number (N_i) of images of the emitter created with the i^{th} reflection. Each image of the emitter is inside an image of the rectangular cavity (Fig. 1). At the beginning, we have only one emitter in the RC, $N_0 = 1$. After one reflection on all the walls, six sources are created outside the RC, $N_1 = 6$ after a second reflection on all the walls, $N_2 = 18$ sources are created. We can show that the i^{th} reflection creates $N_i = 4i^2 + 2$ sources [7]. These sources are outside the RC and can be far away if the number of reflection is high. Their exact positions can be determined with image theory, but we do not need

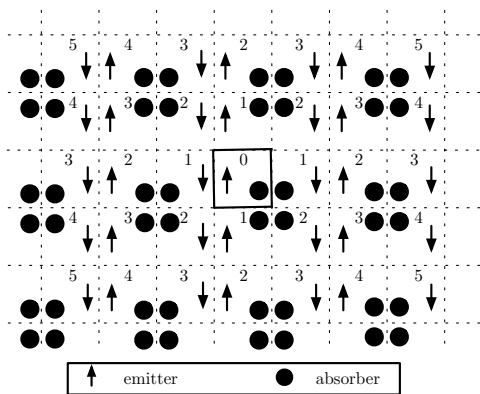


Fig. 1. Image theory model of a rectangular cavity, the number in image cavity indicates the number of reflections

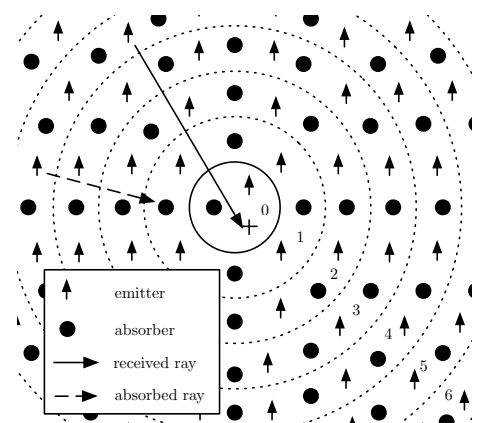


Fig. 2. Concentric spheres model, the number in each circle indicates the number of reflections

such refinements in our study and we will use an approximate relation between the number of reflections and the time. We need to find a typical distance L^1 that would represent the mean distance between two reflections in the chamber. In a rectangular cavity with dimensions l, p, h , this distance L is given by the reverberation distance in acoustics [8]:

$$L = \frac{4V}{S} = \frac{4lph}{2(lp + lh + hp)}. \quad (4)$$

where V is the volume of the chamber and S its surface. Using one distance L to represent the reverberation phenomenon is similar to reducing the problem to one dimension, as if the chamber were spherical. The model is now reduced to concentric spheres with radius iL , where i is the number of reflection (Fig. 2). Between the spheres of radius $(i+1)L$ and iL we have $N_i = 4i^2 + 2$ sources uniformly distributed. The power received in the reverberation chamber after i reflections is the contribution of these N_i sources:

$$P(i) = \frac{N_i R^{2i} E_0^2}{4\pi i^2 L^2} \approx \frac{R^{2i} E_0^2}{\pi L^2} \approx R^{2i} P_0. \quad (5)$$

¹In [7], we used the smallest dimension of the chamber ($h = 2.9$ m). Due to the geometry of our chamber that is very long it did not affect the results. The mean distance ($L \approx 2.74$ m) from acoustic theory seems more rigorous.

We can express the power received as a function of time by using $i \approx t \frac{c}{L}$. We can write:

$$P(t) \approx P_0 R^{2t \frac{c}{L}}. \quad (6)$$

The time constant τ_{ec} for an empty RC can be extracted by using (2) and (6):

$$\tau_{ec} \approx -\frac{L}{2c \ln(R)}. \quad (7)$$

This equation is similar to the acoustic Norris-Eyring equation [8].

A CIR measurement in a given bandwidth is needed to extract τ_{ec} and then to deduce R . In our $8.7 \times 3.7 \times 2.9$ m³ RC, we have $L \approx 2.74$ m, $\tau_{ec} \approx 2.76$ μ s and $R \approx 0.9983$, in the 1 – 2GHz bandwidth.

B. Power Absorption Model

Some definitions first, if we consider an object, the surface of its envelope is noted S_o . When a part of this surface is masked by a wall or another object, we note the remaining visible surface S_v . The average cross section σ of this object is the average apparent surface over 4π steradians. The average absorbing cross section σ_a is the equivalent surface of this object if it were a perfect absorber. The efficiency of the absorbing material is $\eta = \sigma_a/\sigma$.

Matter is imaged with image theory [9], as a result, with an absorber in the RC, an image of this absorber is created in each image cavity (Figs. 1 and 2). In the end there are N_i absorbers created by the i^{th} reflection. These N_i absorbers are uniformly distributed between the spheres of radius $(i+1)L$ and iL . If we consider a perfectly absorbing material, the incident E-field on the material is totally absorbed. The probability $p(i)$ for a ray to be absorbed by an absorbing object with absorbing cross section σ_a is given by:

$$p(i) \approx \frac{(4i^2 + 2)\sigma_a}{4\pi i^2 L^2} \approx \frac{\sigma_a}{\pi L^2}. \quad (8)$$

The probability for a ray from the i^{th} sphere, to reach the inner sphere (the real reverberation chamber, where the measurement is made) is given by:

$$p_m(i) = (1 - p_0) \prod_{j=1}^i (1 - p(j)) \approx \left(1 - \frac{\sigma_a}{\pi L^2}\right)^i, \quad (9)$$

with p_0 the probability of a ray to be absorbed in the real reverberation chamber. This term is neglected in the approximate expression.

The E-field measured in the reverberation chamber can be derived from (3) and (9):

$$E(i) \approx E_0 \left(R \left(1 - \frac{\sigma_a}{\pi L^2}\right)\right)^i. \quad (10)$$

We can write the power as a function of time by using $i \approx \frac{tc}{L}$:

$$P(t) \approx P_0 \left(R \left(1 - \frac{\sigma_a}{\pi L^2} \right) \right)^{2t \frac{c}{L}} \quad (11)$$

$$\approx P_0 \exp \left(\frac{2tc}{L} \left[\ln(R) + \ln \left(1 - \frac{\sigma_a}{\pi L^2} \right) \right] \right) \quad (12)$$

$$\approx P_0 \exp \left(-t \left[\frac{1}{\tau_{ec}} - 2 \frac{c}{L} \ln \left(1 - \frac{\sigma_a}{\pi L^2} \right) \right] \right) \quad (13)$$

and we can extract the time constant τ_a , of the loaded chamber as a function of the absorbing cross section σ_a :

$$\tau_a \approx \frac{\tau_{ec}}{1 - 2 \frac{c}{L} \tau_{ec} \ln \left(1 - \frac{\sigma_a}{\pi L^2} \right)} \quad (14)$$

We can verify that the inverse of the quality factor $Q = 2\pi f_0 \tau_a$ is the sum of the inverse of Q_{ec} , (quality factor of the empty chamber) and the inverse of Q_a (quality factor of the absorbing object in the chamber):

$$\frac{1}{Q} \approx \frac{1 - 2 \frac{c}{L} \tau_{ec} \ln \left(1 - \frac{\sigma_a}{\pi L^2} \right)}{2\pi f_0 \tau_{ec}} \quad (15)$$

$$\frac{1}{Q} \approx \frac{1}{2\pi f_0 \tau_{ec}} - \frac{2c \ln \left(1 - \frac{\sigma_a}{\pi L^2} \right)}{2\pi f_0 L} \quad (16)$$

$$\frac{1}{Q} \approx \frac{1}{Q_{ec}} + \frac{1}{Q_a} \quad (17)$$

It shows that our model of power absorption in the chamber is in agreement with the theory of the quality factor of an RC [5].

C. Absorbing Cross Section

In order to characterize an absorber, we need to extract its absorbing cross section from a measurement of the time constant τ_a . From (14), we can extract σ_a :

$$\sigma_a \approx \pi L^2 \left[1 - \exp \left(\frac{L}{2c} \left(\frac{1}{\tau_{ec}} - \frac{1}{\tau_a} \right) \right) \right] \quad (18)$$

D. Numerical Estimation of σ

The value σ obtained is the average cross section of the absorbing object over 4π steradians [5]. If this cross section is easy to estimate with simple objects like spheres ($\sigma = \pi r^2$), it is not easy to estimate this cross section for objects like rectangular absorbers or pyramidal absorbers. We have developed a numerical method to estimate the mean cross section σ . We use a 3D model of the object. For an incident plane wave with a given elevation and azimuth, we color in black the visible part of the object from the angle of view with the same elevation and azimuth angles and repeat this procedure for every combination of elevation and azimuth angle (180×360 angles). We count the black pixels for every image, after applying a scaling factor to convert pixels in square meter, we compute the average number of pixels to obtain the average cross section σ . Fig. 3 shows an illustration of this technique for an array of pyramidal absorbers for a particular angle of view.

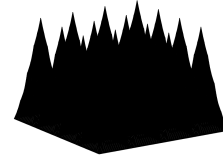


Fig. 3. View from the angle azimuth = 56° and elevation = 16° of a 4×4 pyramidal absorber absorbing cross section

III. MEASUREMENTS AND CHARACTERIZATION OF AN ABSORBING BLOCK

A. Modus Operandi

In the following section, we present the experimental results to validate the theory exposed above. The experiments are made in the RC of our laboratory which has the following dimensions: length (l) 8.7 m, width (p) 3.7 m, and height (h) 2.9 m. The lowest usable frequency of this RC is estimated at 250 MHz [10]. Measurements are performed by using the network analyzer, N5230A, in the 1 GHz and 2 GHz band with a resolution of 20001 points, the maximum length of CIR in time domain is $20 \mu s$. Two horn antennas (1 – 18 GHz) are placed randomly in RC, but well oriented and in a cross-polarization configuration in order to minimize the direct component and obtain a quasi perfect Rayleigh distribution [4], [11]. In the measurement bandwidth, the gain of antennas does not fluctuate too much so all the frequencies are excited with almost the same amount of power. The chamber is loaded gradually with identically rectangular absorbing foams, type Hyfral P150, with the dimensions: $0.6 \times 0.6 \times 0.15 \text{ m}^3$. The total surface of this absorber is $S_o = 1.08 \text{ m}^2$.

Because the measurements are made in a large bandwidth and not for a single frequency, the computed quality factor is a combination of multiple quality factors of each mode excited by the wide band signal of 1 GHz. Previous measurements showed that time delays have a small variation with frequency. Even if the electrical properties of the absorbers may change in the measured bandwidth, the computed absorbing cross section represents an average value in the test band. Moreover, performing the measurements in a large bandwidth, the multiple excited modes act as a stirring mechanism, the use of a supplementary mechanical stirring to create the uniformity of the E-field is not necessary.

B. Absorbing Cross Section of an Absorbing Block in various configurations

Using the configuration presented above, we measure the degree of absorption of one absorber placed in different configurations (Fig. 4). We analyze how the total real surface of absorber influences the average surface of absorption σ_a . In a first case we set the absorber horizontally on the floor of the RC (Fig. 4-(a)). The visible surface of this absorber is $S_v = 0.72 \text{ m}^2$. Fig. 5-(a) is presents the normalized power delay profile of the channel impulse response of the CW signal sent in the bandwidth 1 – 2 GHz. Fig. 5-(b) presents the normalized energy as a function of time. The normalized

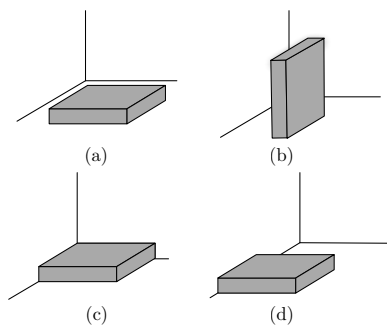


Fig. 4. Configurations of the absorbing block: (a) standing horizontally, (b) standing vertically, (c) in a corner, (d) along an edge

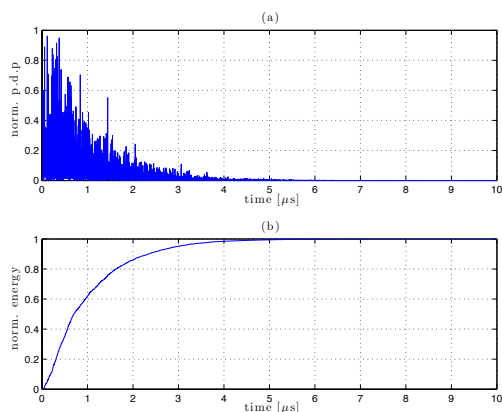


Fig. 5. CIR for a signal of 1 GHz bandwidth when 1 absorber is placed in RC, (a) Normalized power delay profile; (b) Normalized energy

energy follows an exponential curve, and we can easily extract $\tau_a \approx 1.135 \mu\text{s}$. From (18) and with τ_{ec} (the included losses are those from the chamber walls, the antennas, the cables and any other leakage), we find the average absorbing cross section as $\sigma_a = 0.0557 \text{ m}^2$. Obviously, we obtain a smaller time delay than in an empty cavity. With a higher degree of absorption, less energy will arrive at reception.

The next test uses the same absorber but this time is set vertically on its edge on the floor of RC (Fig. 4-(b)). The visible surface is now $S_v = 0.99 \text{ m}^2$ (a 37% increase). Measuring as before the time delay and the average absorbing cross section, we obtain $\tau_a = 0.975 \mu\text{s}$ and $\sigma_a = 0.0713 \text{ m}^2$. The equivalent surface σ_a is greater than before with 42 %. As a result, the time delay decreases because more rays are absorbed. There is no proportional relation between the visible surface and the absorbing cross section. With the help of the method presented in section II-D this aspect can be studied.

We test more configurations in which the absorber is placed in different positions in the chamber. One configuration uses one absorber placed in a corner of the RC (Fig. 4-(c)), only three of the six sides are visible and the visible surface in this case is $S_v = 0.54 \text{ m}^2$. We obtain $\tau_a = 1.4 \mu\text{s}$ and $\sigma_a = 0.0379 \text{ m}^2$. Changing the position of the absorber on an edge of the RC (Fig. 4-(d)), the total visible surface becomes $S_v = 0.63 \text{ m}^2$ and we have $\tau_a = 1.29 \mu\text{s}$ and $\sigma_a = 0.0444 \text{ m}^2$.

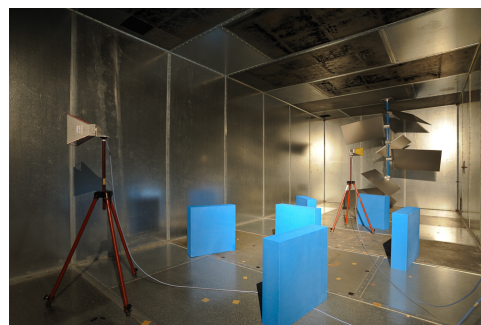


Fig. 6. Experimental configuration with $N = 6$ pieces of absorbers

We gather these results and in Table I. We see clearly that

TABLE I
MEASUREMENTS RESULTS FOR DIFFERENT CONFIGURATIONS

Position	τ_a (μs)	σ_a (m^2)
Horizontally, Fig. 4-(a)	1.135	0.0557
Vertically Fig. 4-(b)	0.975	0.0713
In a corner, Fig. 4-(c)	1.400	0.0379
Along an edge, Fig. 4-(d)	1.290	0.0444

even the placement of one absorber impacts the time delay. Depending on how the absorbers are placed in the chamber, if they are not illuminated evenly, not all the absorption surface is used properly.

C. Simulation with N Absorbers

We make another set of measurements to test if the equivalent surface is detected when the number of absorbers is increased. Consecutively, we charge the RC with a different amount of absorbers, and for each configuration we compute the equivalent absorption surface and time delay. We set the absorbers vertically and place them randomly in the RC. We try to put absorbers far from each other to limit shadowing effects with respect to incoming waves (Fig.6).

Using the absorbing cross section determined for the case when one absorber is used, $\sigma_a = 0.0713 \text{ m}^2$, we predict the time delay for N absorber, with N varying from 1 to 20. The simulated time delays are compared with measurements in Table II. The two time delays are also presented in Fig. 7. Fig. 8 compares the absorbing cross section mea-

TABLE II
SIMULATED AND MEASURED TIME DELAY FOR N ABSORBERS

N	Sim. τ_a (μs)	Meas. τ_a (μs)	τ_a relative error
0	-	2.754	-
1	0.975	0.975	-
2	0.591	0.574	-3%
3	0.424	0.459	8%
4	0.330	0.374	12%
5	0.271	0.317	15%
10	0.141	0.204	31%
15	0.095	0.135	30%
20	0.071	0.110	35%

sured with N absorbers with the simulated absorbing cross

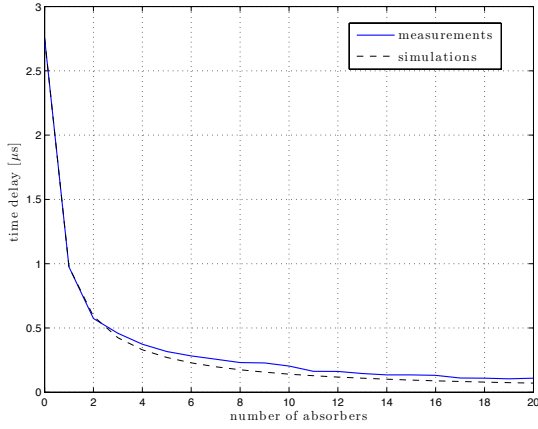


Fig. 7. Simulated and measured time delays for a number of absorbers from 1 to 20

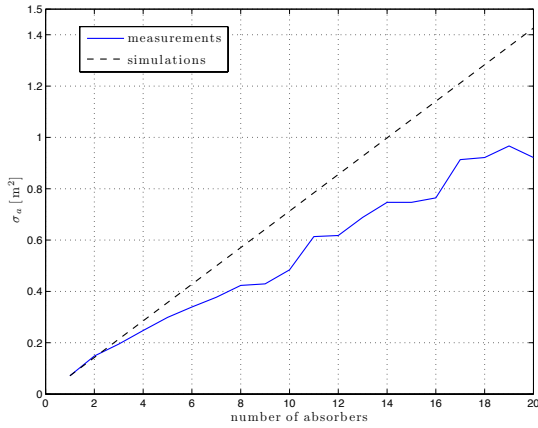


Fig. 8. Simulated and measured average cross sections for a number of absorbers from 1 to 20

section ($N \times 0.0713 \text{ m}^2$).

We can note a deviation between simulations and measurements of the average absorbing cross section σ_a (or the time constant τ_a) when the number of absorbers in the RC increases. One reason could be the uncertainty of measurements another could be a bias between the estimation and the true value. Even if some errors in measurement and in the estimation of the average surface exist, our supplementary measurements showed that in the presence of a high number of absorbers confined in a limited volume, the total absorption surface σ_a can not be considered anymore as a simple summation of each individual equivalent surface. Because some absorbers overshadow others, the total absorption surface is reduced. Rigorously, absorbing objects in an RC cannot be regarded as independent absorbing quantities. If the number of absorbing objects is too high, we have to characterize the absorbers as an unique absorbing object. We can push a little more the analysis to characterize the material used in the absorber.

IV. MATERIAL CHARACTERIZATION

In this section we will simulate the ideal absorbing cross section σ by using the method presented in section II-D. The

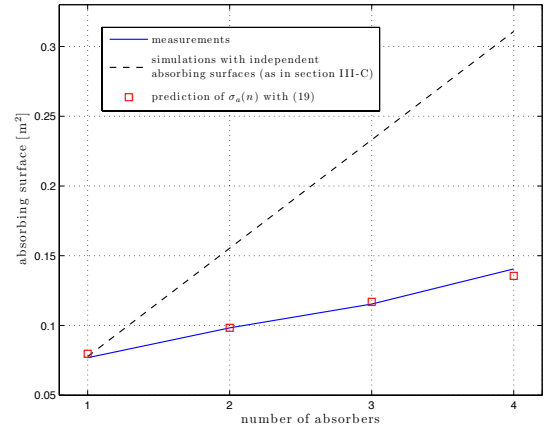


Fig. 9. Simulated (by summing independently the absorbing surfaces) and measured average cross sections for a number of absorbers from 1 to 4 placed on a polystyrene cube, and empirical simulation $\sigma_a(n)$

ratio between the simulated value (σ) and measurements (σ_a) gives a numerical value of the efficiency of the absorbing material (η %).

A. Pilling Up Absorbers

To increase the surface of absorption the absorbers have to be placed in air. We use a polystyrene cube ($0.6 \times 0.6 \times 0.6 \text{ m}^3$) as a support to put the absorbers on it. Even if this polystyrene support is not perfectly transparent, it has a very little degree of absorption. Measuring its absorption surface, we find $\sigma_a = 0.0025 \text{ m}^2$. This absorption surface is really small compared with the average ideal absorption surface of one absorber. We consider the losses of the polystyrene support as part of the chamber losses ($\tau_{ec} \approx 2.588 \text{ } \mu\text{s}$). We place successively 4 absorbers on the cube one on top of the other. The measurements results compared with simulations for the case where all the absorbers are placed independently in the RC (section III-C) are presented in Fig. 9 (dotted line). For each overlapping of absorbers we lose a visible surface of 0.72 m^2 . In this configuration the average absorption cross section can not be predicted as the sum of independent surfaces anymore.

In order to simulate this configuration properly, we use the method presented in section II-D to estimate σ for each configuration. These kind of simulations are needed especially for complex shapes for which an analytic solution is very hard to be found. We present the results in Table III. We can clearly see that the relative surface for different numbers of absorbers found in measurements is respected in our simulations. The ratio between the measured cross section σ_a and the simulated cross section σ is given in the third column. This factor contains the properties of the material the absorber is made with.

The absorption efficiency remains in the same range (25-27%), it characterizes the absorption of the material in the RC and it should not change no matter how the absorbers are placed in the RC. From the 3D simulations results and with η ,

TABLE III
MEASUREMENTS AND SIMULATION RESULTS FOR A PILE OF n ABSORBERS

n	σ_a (m ²)	σ (m ²)	Material abs. efficiency, η (%)
1 (0.6 × 0.6 × 0.15 m ³)	0.077	0.305	25.3
2 (0.6 × 0.6 × 0.3 m ³)	0.098	0.377	26.0
3 (0.6 × 0.6 × 0.45 m ³)	0.115	0.448	25.7
4 (0.6 × 0.6 × 0.6 m ³)	0.141	0.520	27.1

we can deduce an empirical prediction of σ_a in our chamber as a function of the number of absorbers ($n > 0$), presented in Fig. 9:

$$\sigma_a(n) \approx \eta(0.0716n + 0.235). \quad (19)$$

B. 4×4 Pyramidal Absorber

The method used to simulate the average surface is even more useful if the shape of the object is more complicated. We test this method with a 4 × 4 pyramidal absorber (Fig. 3). We use the pyramidal absorber in two configurations in which it is placed either directly on the metallic floor of the RC or on the polystyrene cube. Even if the total surface of pyramidal absorber is much higher than the surface of the rectangular absorber, it will encounter a high degree of shadowing of one component pyramid to another. In addition, pyramidal absorbers include a secondary type of absorption caused by successive reflections on the edges of pyramids. The total surface of the pyramidal absorber is $S_o = 2.4156$ m². As before the absorption of the polystyrene cube is included in the losses of RC. From measurements we obtain for the empty cavity, $\tau_{ec} \approx 2.594$ μ s. When using the pyramidal absorber on the block we find $\tau_a \approx 0.706$ μ s, while the average absorption surface measured σ_a is 0.110 m². Setting the absorber on the floor of RC, the visible surface S_v is reduced to 2.056 m². Because less rays are absorbed, the time delay increases at $\tau_a \approx 0.871$ μ s, corresponding to an average absorption surface of $\sigma_a = 0.082$ m². We simulate this shape in order to find an equivalent surface in both configurations. We fill in the Table IV.

TABLE IV
MEASUREMENTS AND SIMULATION RESULTS

Configuration	σ_a (m ²)	σ (m ²)	Material abs. efficiency, η (%)
On polystyrene cube	0.110	0.562	19.6
On the RC floor	0.082	0.421	19.5

For both cases we find almost the same efficiency. This efficiency is not as good as for the rectangular absorbers. It might be due to electromagnetic and geometrical properties, pyramidal absorbers being more efficient with normal radiation.

With the methods presented above we can identify the degree of absorption of an object by estimating its equivalent absorption surface. It allows to compare different absorption materials. Moreover we can estimate the quality factor (respectively the time delay) as a function of the degree of absorption η . Inversely, by knowing the shape of an object and the absorbing efficiency of its materials, we can predict its effect on the loading of the chamber.

V. CONCLUSION

In this article we present a simple power absorption model in an RC. With time domain measurements, this model allows to characterize the absorbing cross section of one object and to deduce the effect of N objects on the quality factor or the time response τ as far as we can consider that the objects are independent. The bandwidth can be reduced to examine more precisely the behavior of the absorber around a given frequency. A frequency approach is possible but it will involve the use of the mechanical stirrer to determine Q or τ and the measurement duration would be increased drastically.

We propose a practical approach to determine numerically the average cross section of any geometry. This average cross section allows to determine the absorption efficiency of the material used in the absorber.

These two aspects are useful to control the quality factor or the power delay profile with precision in a reverberation chamber in order to make consistent EMC testings or channel emulations.

ACKNOWLEDGEMENTS

This work was partly supported by the French Ministry of Defense DGA (Direction Générale de l'Armement) and also partly supported by the French Research Agency (ANR) in the frame of the METAPHORT project.

REFERENCES

- [1] CIS/A, "IEC 61000-4-21: Electromagnetic compatibility (EMC) - part 4-21: Testing and measurement techniques - reverberation chamber test methods," IEC, Tech. Rep., 2003.
- [2] O. Lunden and M. Backstrom, "Absorber loading study in FOI 36.7 m³ mode stirred reverberation chamber for pulsed power measurements," in *Electromagnetic Compatibility, 2008. EMC 2008. IEEE International Symposium on*, 2008, pp. 1–5.
- [3] S. Cantalice, G. Fontgalland, R. Freire, E. Richalot, and S. Barbin, "Influence of an asymmetrically positioned load in a reverberation chamber," in *Instrumentation and Measurement Technology Conference, 2009. I2MTC '09. IEEE*, May 2009, pp. 1616–1619.
- [4] C. Holloway, D. Hill, J. Ladbury, P. Wilson, G. Koepke, and J. Coder, "On the use of reverberation chambers to simulate a rician radio environment for the testing of wireless devices," *Antennas and Propagation, IEEE Transactions on*, vol. 54, no. 11, pp. 3167–3177, 2006.
- [5] C. Holloway, D. Hill, J. Ladbury, and G. Koepke, "Requirements for an effective reverberation chamber: unloaded or loaded," *Electromagnetic Compatibility, IEEE Transactions on*, vol. 48, no. 1, pp. 187–194, 2006.
- [6] J. Coder, J. Ladbury, C. Holloway, and R. K.A., "Examining the true effectiveness of loading a reverberation chamber," in *Electromagnetic Compatibility, 2010. EMC 2010. IEEE International Symposium on*, 2010, pp. 1–6.
- [7] E. Amador, C. Lemoine, P. Besnier, and A. Laisné, "Reverberation chamber modeling based on image theory: Investigation in the pulse regime," *Electromagnetic Compatibility, IEEE Transactions on*, vol. 52, no. 4, pp. 778–789, 2010.
- [8] T. Rossing and N. Fletcher, *Principles of vibration and sound*. New York: Springer-Verlag, 2004, ch. 11, pp. 258–259.
- [9] R. Harrington, *Time-Harmonic Electromagnetic Fields*. New York: McGraw-Hill Book Company, 1961, pp. 103–105.
- [10] C. Lemoine, P. Besnier, and M. Drissi, "Investigation of reverberation chamber measurements through high-power goodness-of-fit tests," *IEEE Transactions on Electromagnetic Compatibility*, vol. 49, no. 4, pp. 745–755, 2007.
- [11] C. Lemoine, E. Amador, and P. Besnier, "On the K-factor estimation for rician channel simulated in reverberation chamber," *Antennas and Propagation, IEEE Transactions on*, vol. 59, no. 3, pp. 1003–1012, March 2011.